On-tissue Chemical Derivatization of Catecholamines Using 4-(*N*-methyl) Pyridinium Boronic Acid for ToF-SIMS and LDI-ToF Mass Spectrometry Imaging

***Ibrahim Kaya*[1,2,3], *Steffen M. Brülls*[4], *Johan Dunevall*[1,3], *Eva Jennische*[5], *Stefan Lange*[5], *Jerker Mårtensson*[4], *Andrew G. Ewing*[1,3], *Per Malmberg*[3,4], *John S. Fletcher*[1,3*]**

[1] Department of Chemistry and Molecular Biology, University of Gothenburg, Kemivägen 10, 405 30 Gothenburg, Sweden

[2] Department of Psychiatry and Neurochemistry, Sahlgrenska Academy at the University of Gothenburg, Mölndal Hospital, House V3, 43180 Mölndal, Sweden

[3] The Gothenburg Imaging Mass Spectrometry (Go: IMS) Platform, University of Gothenburg and Chalmers University of Technology, Gothenburg 412 96, Sweden

[4] Department of Chemistry and Chemical Engineering, Chalmers University of Technology, 412 96 Gothenburg, Sweden

[5] Institute of Biomedicine, University of Gothenburg, Gothenburg 413 90, Sweden

***Corresponding Author**

John S. Fletcher

Department of Chemistry and Molecular Biology, University of Gothenburg, Analytical Chemistry, SE-412 96, Gothenburg, Sweden

john.fletcher@chem.gu.se;

+46-76 622 91 05

ABSTRACT

The analysis of small polar compounds with ToF-SIMS and MALDI-ToF-MS have been generally hindered by low-detection sensitivity, poor ionization efficiency, ion suppression, analyte in-source fragmentation and background spectral interferences from either MALDI matrix and/or endogenous tissue components. Chemical derivatization has been a well-established strategy for improved mass spectrometric detection of many small molecular weight endogenous compounds in tissues. Here, we present a devised strategy to selectively derivatize and sensitively detect catecholamines with both secondary ion ejection and laser desorption ionization strategies which are used in many imaging mass spectrometry (IMS) experiments. Chemical derivatization of catecholamines was performed by a reaction with a synthesized permanent pyridinium cation-containing boronic acid molecule, 4-(*N*-methyl) pyridinium boronic acid, through boronate ester formation (boronic acid-diol reaction). The derivatization facilitates their sensitive detection with ToF-SIMS and LDI-ToF mass spectrometric techniques. 4-(*N*-methyl) pyridinium boronic acid worked as a reactive matrix for catecholamines with LDI and improved the sensitivity of detection for both SIMS and LDI while the isotopic abundancies of the boron atom reflects a unique isotopic pattern for derivatized catecholamines in MS analysis. Finally, the devised strategy was applied, as a proof of concept, for on-tissue chemical derivatization and GCIB-ToF-SIMS (down to 3 μm per pixel spatial resolution) and LDI-ToF mass spectrometry imaging of dopamine, epinephrine, and norepinephrine in porcine adrenal gland tissue sections. MS/MS using collision-induced dissociation (CID)-ToF-ToF-SIMS was subsequently employed on the same tissue sections after SIMS and MALDI mass spectrometry imaging experiments which provided tandem MS information for the validation of the derivatized catecholamines in situ. This methodology can be a powerful approach for the selective and sensitive ionization/detection and spatial localization of diol-containing molecules such as aminols, vic-diols, saccharides and glycans along with catecholamines in tissue sections with both SIMS and LDI/MALDI-MS techniques.

INTRODUCTION

Knowledge of the spatial distribution profiles of endogenous metabolites within mammalian tissues can provide a basis for the understanding of their roles in local biological and metabolic processes. Neurotransmitters (NTs), including catecholamines are critical chemical messengers and have been implicated in the regulation of several biological processes and behavior.[1-3] Therefore, sensitive and selective analytical techniques are needed to determine the spatial localizations of these molecules in tissues which would help to construe their roles in physiological and/or pathophysiological processes.

Imaging mass spectrometry (IMS) allows label-free spatially-correlated mass spectrometric analysis for the simultaneous interrogation of a wide-range of endogenous biomolecules including proteins[4,5], peptides[6,7], lipids[8,9] and small metabolites[10] on tissue sections. Most IMS experiments use either laser desorption/ionization (LDI) or secondary ion mass spectrometry (SIMS) ionization strategies.[11,12] Tissue sections are raster scanned either with primary ion beams or energetic laser pulses for SIMS and LDI respectively and the resulting spectra from the pixel points are analyzed and used to generate ion distribution images of biomolecules, fragments of molecules or elements across the surface of tissue sections and cells. Although the advent of IMS allowed accurate determination of low-molecular-weight metabolites including NTs over tissue sections at high-spatial resolutions,[11,13] the analysis of small polar compounds with ToF-SIMS and MALDI-ToF-MS has generally been hindered by low-detection sensitivity, poor ionization efficiency, ion suppression, analyte in-source fragmentation and background spectral interferences from either MALDI matrix and/or endogenous tissue components.[14]

Regarding MALDI-TOF-MS, optimal selection of MALDI matrix and/or careful optimization of analysis parameters may be used to minimize the matrix-derived interferences and improve the sensitivity.[6,9,15,16] However, this can be restricted due to the fact that all the MALDI matrix molecules have distinct physicochemical properties which upon laser irradiation results in distinct ionization mechanisms and laser desorption/ionization dynamics.[17-19] The use of high

mass-resolution analyzers and MS/MS analysis can aid in the detection of some compounds.[20,21] For example, a combination of C_{60} primary ion beam with an FT-ICR instrument was used to achieve a spatial resolution of ~40 μm and 100,000 mass-resolving power when imaging cholesterol in a rat brain section.[21] However, low sensitivity even at large pixel sizes and long pixel acquisition times limits their regular use for acquiring large images. Therefore, there is need for new strategies to improve either the sensitivity and/or specificity of the IMS analysis of small polar compounds. Recently, Ellis et al. combined a laser post-ionization technique[22] with high mass-resolving Orbitrap mass spectrometer which yielded enhanced sensitivity, selectivity and chemical coverage of lipids for MALDI-IMS[23] and can potentially be used for accurate detection of NTs as well. Moreover, Passarelli et al. introduced a hybrid mass analyzer design which allows the user to switch between high-speed ToF imaging and high mass-resolving power and MS/MS capability of a Q Exactive HF Orbitrap and accurate SIMS detection of NTs such as dopamine, serotonin, γ-aminobutyric acid (GABA) at sub-cellular spatial resolutions has been reported.[24]

Another approach to increase selectivity and/or sensivity for mass spectrometry analysis of small polar compounds including NTs is in-situ chemical derivatization.[14] A selective derivatization of analyte molecules which enhances ionization and/or desorption yields can enable specific detection of NTs with ToF-SIMS and LDI-ToF mass spectrometry.

Boronic acids readily react with biological molecules containing polyhydroxy motifs, which enables them to react with diols to form five-membered boronate esters.[25] This feature has been utilized for the recognition and sensing of polyhydrodxy group-containing molecules including saccharides[26] and catecholamines.[27,28] Catecholamines such as epinephrine, norepinephrine and dopamine are low-molecular-weight polar compounds containing a catechol group (*ortho* isomer of dihydroxybenzene) in their molecular structure. Here we present a selective method for chemical derivatization of catecholamines by reaction with a permanent pyridinium cation-containing boronic acid molecule, 4-(*N*-methyl) pyridinium boronic acid, which facilitates their specific and sensitive detection with ToF-SIMS and LDI-ToF mass spectrometry. Finally, the devised strategy was applied, as a proof of concept, for

on-tissue chemical derivatization and ToF-SIMS and/or LDI-ToF mass spectrometry imaging of dopamine, epinephrine, norepinephrine in porcine adrenal gland tissue sections.

EXPERIMENTAL SECTION

Chemicals and Reagents. All chemicals were pro-analysis grade and obtained from Sigma-Aldrich (Stockholm, Sweden unless otherwise specified. TissueTek optimal cutting temperature (OCT) compound was purchased from Sakura Finetek (AJ Alphen aan den Rijn, the Netherlands). The *d*H2O was obtained from a Milli-Q purification system (Merck Millipore, Darmstadt, Germany).

Synthesis of 4-(*N*-methyl) pyridinium boronic acid iodide. A modified version of previously-described protocol was used for the synthesis of 4-(*N*-methyl) pyridinium boronic acid Iodide compound.[29] The experimental procedure was performed as follows. 155 mg of 4-pyridyl boronic acid pinacol ester (1 equiv., 0.81 mmol) was dissolved in 15 ml of dry acetonitrile (ACN) under inert nitrogen atmosphere, 0.26 ml methyl iodide (5 equiv., 4.1 mmol) was added and the solution heated up to 80°C for 6 h. Acetonitrile was removed under reduced pressure. The yellow colored intermediate was dissolved in 10 ml water with the addition of 1M hydrochloric acid (2 ml) and stirred for one hour at RT. After one hour, the water phase was washed with tetrahydrofuran to remove pinacol. Water was removed under reduced pressure and the product was precipitated from MeOH/diethylether resulting in a pale, white-colored product (173 mg). The details of the synthesis and NMR spectra are provided in Supporting Information Figure S-1, 2, 3,4, 5. High Resolution Mass Spectrometry (HRMS) analysis of 4-(*N*-methyl) pyridinium boronic acid (4-(*N*-Me)$Py^+B(OH)_2$) was performed using LC-ESI-QTOF-MS. The signal of the molecular ion $[M]^+$ is detected at m/z 138.07. The m/z value of the molecule and its isotopic pattern are in agreement with the theoretical ones (Supporting Information Figure S-6).

Animals, Tissue Sampling and Sectioning.

The pig adrenal glands were obtained from animals after termination of control experiments for other ethically approved experiments. The adrenal glands were rapidly frozen in liquid nitrogen. The material was kept at -80 °C until sectioning. Frozen tissue sections (10 µm thick) were cut in a cryostat microtome (Leica CM 1520, Leica Biosystems, Nussloch, Germany) at 20 °C, and collected on indium tin-oxide (ITO) coated glass slides (Bruker Daltonics, Bremen, Germany) and stored at 80 °C.

Sample Preparation and Matrix Application

Prior to on-tissue derivatization, tissue sections were thawed in a desiccator for ~30 min under reduced pressure (SpeedVac, Eppendorf, Hamburg, Germany). For teaching of the navigation points in Flex Imaging v3.0 software, a glass cutter pen (Starwalker, Montblanc, Germany) was used to leave sharp-edged cross signs on the indium tin oxide (ITO) coated glass supporting the tissue sections. The sections were scanned in a slide scanner (PathScan Enabler IV, Electron Microscopy Sciences, Hatfield, PA) to visualize the tissue regions. On tissue derivatization was performed by applying the 4-(*N*-methyl) pyridinium boronic acid iodide derivatizing compound using a TM Sprayer (HTX Technologies, Carrboro, NC) combined with a HPLC pump (Shimadzu LC-10ADVP, Kyoto, Japan). Before every spraying experiment, the drain valve was opened and ~10 min purge was applied followed by running the pump with 1.5 ml/min flow with an open valve for ~5 minutes. Then, the pump was kept running at 100 µl/min using a 70% ACN pushing solvent with isocratic pressure (at ~40 bar) for ~3h. 12 mg/ml 4-(N-methyl) pyridinium boronic acid iodide in 60% ACN/H_2O solution was sprayed over the tissue sections using instrumental parameters including nitrogen flow of 10 psi, spray temperature of 75 °C, nozzle height of 40 mm, fifteen passes with offsets and rotations, and a "spray velocity" of 1300 mm/min.

ToF-SIMS, CID-ToF-ToF-SIMS-MS/MS, ToF-SIMS Imaging. ToF-SIMS analysis was performed using an Ionoptika J105 instrument (Ionoptika Ltd, UK) that has been described in detail elsewhere.[30,31] Briefly, the instrument employs a linear buncher to compress a stream of

secondary ions to a time focus at the entrance to a reflectron mass analyser. Compared to conventional ToF-SIMS instruments the mass spectrometry is decoupled from the pulsing of the primary ion beam and sample topography. The J105 in Gothenburg is currently equipped with a 40 kV C_{60} ion gun and a 40 kV gas cluster ion gun that fires ionized gas clusters produced by the expansion of pressurized gas as it enters an expansion chamber at the rear of the gun. In this study clusters of CO_2 we used. Following ionization by electron impact the clusters are size selected using a Wien filter. For all experiments $(CO_2)_{6k}^+$ ions were selected (+/- 2000). Such ion beams produce significant increases in intact molecular signal, particularly lipids, compared to traditional primary ion beams and as such have been used to good effect for imaging a range of different cell and tissue samples.

MS/MS was performed, as described and demonstrated previously, [38-40] in a ToF-ToF configuration with collisional-induced dissociation occurring in a short, field free region between the buncher and the reflectron where collision gas (N_2 in this case) is injected. Precursor ion energies range from approximately 0.5-5 keV depending on the position of the ion in the buncher when the buncher accelerating field is applied.

Imaging SIMS uses a combination of beam and sample scanning where for small areas of analysis, <1200 × 1200 μm^2, the ion beam is scanned from pixel to pixel over the sample and for larger areas a series of these ion beam scans are produced at different analysis stage positions to create a series of “tiles” that are combined in the acquisition software to produce a mosaic image. The focus of the ion beam is continuously variable down to the minimum spot size which for this GCIB is 2-3 μm. The specific image dimensions, pixel sizes and primary ion dose densities for each image analysis are specified in the corresponding figure captions.

Sphingomyelin lipid (SM (36:1), $[M+Na]^+$ m/z 753.5), was assigned based on the curated records in the LIPID MAPS database (Nature Lipidomics Gateway, www.lipidmaps.org).

LDI-ToF-MS, LDI-ToF-IMS.

LDI-MS and LDI-IMS were performed using an Ultraflextreme MALDI-TOF/TOF mass spectrometer[41] equipped with a SmartBeam II Nd:YAG/355 nm laser[42] operating at 1 kHz (Bruker Daltonics, Bremen, Germany). Profiling and imaging data acquisitions were performed in reflective (reflectron) positive ion mode under optimized delay extraction conditions in a mass range of 0-1000 Da. Imaging mass spectrometry data were collected using 100 laser shots/per pixel point with a source acceleration voltage of 25kV. The laser focus was set to large and small for 100 µm and 30 µm raster width analysis, respectively. The laser power was adjusted for high desorption ion yields and was kept stable throughout the experiments. Image data were reconstructed and visualized using Flex Imaging v3.0 (Bruker Daltonics, Bremen, Germany). Calibration of the spectra was performed based on the ion of the reactive matrix molecules, 4-(*N*-Me)$Py^{+}B(OH)_2$.

H&E Staining

Consecutive adrenal gland tissue sections were fixed in methanol for 1 min. After drying the, the sections were immersed in Harris hematoxylin (Histolab Products AB, Gothenburg, Sweden) for 45 seconds, rinsed in water and immersed in 0.2% eosin in ethanol (Histolab Products AB, Gothenburg, Sweden) for 30 seconds. The stained sections were rapidly dehydrated in ethanol and mounted in DP mounting solution (BDH chemicals). The sections were scanned using a slide scanner (NanoZoomer SQ, Hamamatsu Photonics, Japan) and the areas corresponding to the area used for imaging MS experiments were captured.

RESULTS AND DISCUSSION

Selective Chemical Derivatization of Catecholamines using 4-borono-N-methylpyridinium Iodide for ToF-SIMS and LDI-ToF Mass Spectrometry Detection.

Chemical derivatization is a well-established strategy to increase the selectivity and/or sensitivity for the mass spectrometry analysis of small polar compounds including catecholamines.[14,43-46] For an ideal chemical derivatization, a characteristic bond-forming reaction is required between the analytes and derivatizing compounds which should further

enable their specific and sensitive ionization via laser desorption and secondary ion ejection and mass spectrometric detection.

Although the fundamental factors affecting selectivity, ionization efficiency, sensitivity, mass resolution, and reproducibility are still not fully understood in MALDI, a two-step model has been widely suggested for the ionization mechanisms, i.e. 1) the initial ion formation which includes the analytes charged in the solution and/or formed by the reaction with matrix ions in the solid-state sample which are then laser-ablation ejected as the ion-containing solid state clusters and evaporated to free the ions according to the cluster model[47,48] and 2) ion-molecule reactions in the laser desorbed plume which involves complex competing charge generation and transfer processes[49] depending on the distinct physicochemical properties of matrix and analyte molecules as well as their interactions with laser pulses.[17-19] In SIMS, ions and neutrals are released from the surface as single atoms, molecules or as a part of large clusters when they have adequate kinetic energy which results from the impact of primary ions and transfer of the primary ion energy to the sample surface.[50] Therefore, for both LDI and SIMS ionization, a permanent charge on the analyte molecules would be advantageous for their effective detection with mass spectrometry.

Catecholamines are organic compounds that have a catechol (1,2-benzene diol) and a side-chain amine in their molecular structure. We devised a strategy to derivatize the catecholamines from their catechol-side by utilizing the high-affinity binding of boronic acids with diol moieties through boronate ester formation.[25] For that, 4-(*N*-methyl) pyridinium boronic acid iodide was synthesized (Figure 1) as a derivatization agent for the following reasonings: (1) Boronic acid containing compounds readily react with diol groups in aqueous solutions and have a strong association constant with catechols. [25,51] 2) The unique isotopic pattern of the boron atom (^{10}B and ^{11}B natural abundance of 19.9 and 80.1%, respectively)[52] reflects a selective isotopic pattern of the ion peak of the derivatized compound.[53] 3) The acidity of pyridinium cation in the molecule's structure makes the boronic acid more reactive[29,54] and this results in more stable boronate ester formation upon reaction with catechols.[54] 4) N-

methylation of the pyridine compound results in a red shift in the UV absorption of the compound which can shift the absorption range of the boronate ester molecule towards to wavelength of the nitrogen/337 nm and Nd:YAG/355 nm lasers which are commonly used in LDI instruments. 5) The 4-(N-methyl) pyridinium group of the compound both provides a permanent positive charge for the sensitive detection of the derivatized compounds with both LDI-ToF-MS and ToF-SIMS and increase the solubility of the compound in aqueous solutions which makes it well suited for imaging mass spectrometry applications.

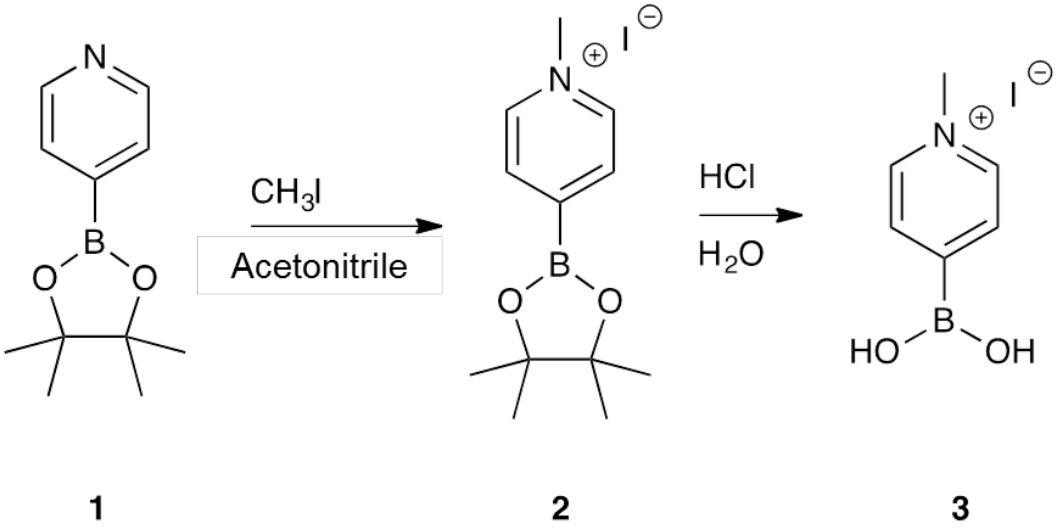

Figure 1. Reaction scheme for the synthesis of 4-(N-methyl) pyridinium boronic acid (4-(*N*-Me)$Py^{+}B(OH)_2$) iodide.

A simple reaction scheme (Figure 1) was used for the synthesis of 4-(*N*-methyl) pyridinium boronic acid (4-(*N*-Me)$Py^{+}B(OH)_2$) starting from the N-methylation of initial compound, 4-pyridineboronic acid pinacol ester (Figure 1-1) to obtain a pyridinum cation which yields 4-(N-methyl) pyridinium boronic acid pinacol ester (Figure 1-2). This was followed by deprotecting the pinacolated boronic acid group to obtain a pyridinium-cation containing boronic acid compound which is 4-(*N*-methyl) pyridinium boronic acid iodide (Figure 1-3). The reaction products were analyzed with LDI-ToF-MS (Figure 2a, b) and MS/MS analysis of the final product was performed with CID-ToF-ToF-SIMS (Figure 2c). 4-(N-methyl) pyridinium boronic

acid pinacol ester (4-(*N*-Me)$Py^+B(OC_3H_6)_2$, m/z 220.0) (Figure 2a) and 4-(N-methyl) pyridinium boronic acid (4-(*N*-Me)$Py^+B(OH)_2$ m/z 138.0) (Figure 2b) were identified by their mass/charge ratios and specific isotopic patterns which are in agreement with theoretical ones.

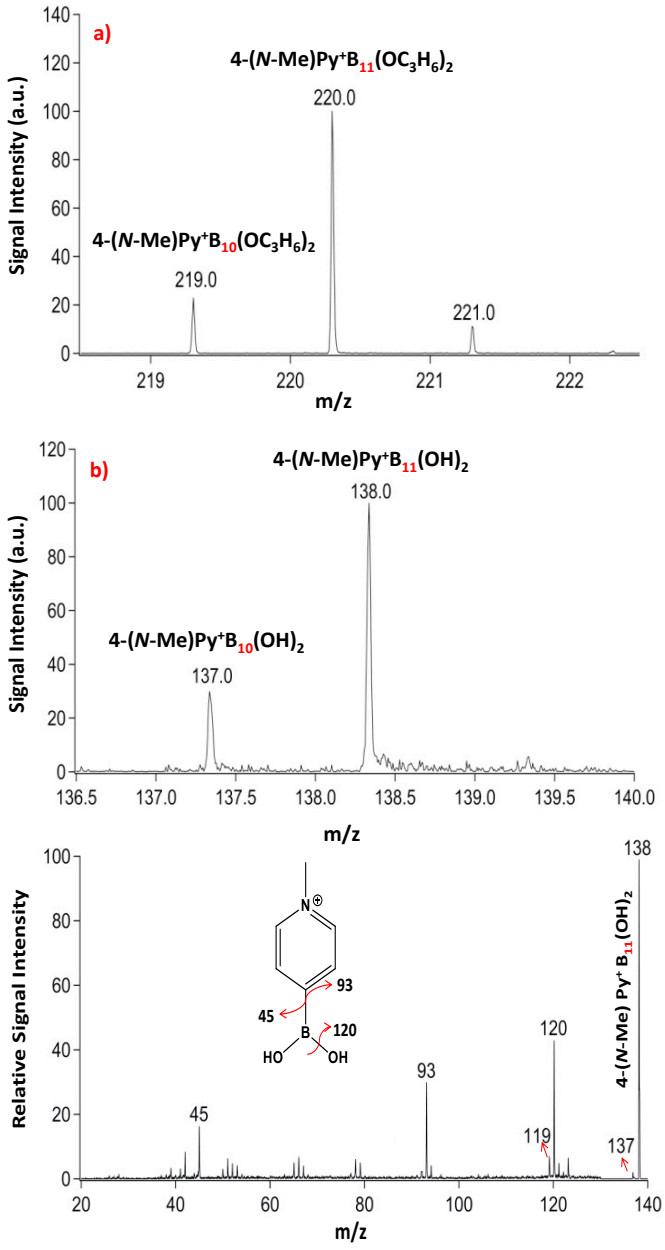

Figure 2. MALDI-ToF-MS spectra of a) 4-(*N*-methyl) pyridinium boronic acid pinacol ester (4-(*N*-Me)$Py^+B(OC_3H_6)_2$, m/z 220.0) iodide and b) 4-(*N*-methyl) pyridinium boronic acid (4-(*N*-Me)$Py^+B(OH)_2$, m/z 138.0) iodide in reflective positive ion mode. c) MS/MS spectra and proposed fragmentation pathway for 4-(*N*-methyl) pyridinium boronic acid (4-(*N*-Me)$Py^+B(OH)_2$) obtained with CID-ToF-ToF-

SIMS in positive ion mode. The product ion region of the MS/MS spectrum was multiplied up by a factor of 50.

To assess the feasibility of 4-(N-methyl) pyridinium boronic acid (4-(*N*-Me)$Py^+B(OH)_2$) compound to be used as a derivatizing agent for catecholamines, solutions of catechol, dopamine, epinephrine and norepinephrine (Figure 3a) were mixed with (4-(*N*-Me)$Py^+B(OH)_2$, spotted on an ITO coated glass microscope slide and left to react. The dried spots were analyzed with LDI-ToF-MS and GCIB-ToF-ToF-SIMS which yielded the ions of corresponding boronate esters resulting from the reaction of boronic acid with catechol groups in catecholamines (Supporting Information Figure S-7,8). It is noteworthy that LDI-ToF-MS analysis worked without the use of a UV-desorption/ionization enhancing ‘’matrix’’ compound. This suggests that the 4-(N-methyl) pyridinium boronic acid functions as a ‘’reactive matrix’’ for diols. UV-VIS spectroscopy analysis revealed the UV absorption maxima of the 4-(N-methyl) pyridinium boronic acid pinacol ester (4-(*N*-Me)$Py^+B(OC_3H_6)_2$) to be 358 nm (in 60% ACN/H_2O) which is close to the 355 nm wavelength of the SmartBeam II (frequency tripled) Nd:YAG laser[42] (Supporting Information Figure S-9) used in our LDI-ToF-MS experiments. It should be noted that the dried crystals in the vacuum will have a broader UV absorption band due to increased scattering in solid state compared to dissolved compound in solution.[17] The use of 4-(*N*-methyl) pyridinium boronic acid as a reactive matrix for catechols also helps to diminish the spectral interferences from matrix clusters (depending on the physicochemical nature of the molecule) in low-mass ranges (typically, ≤ 500 Da.).

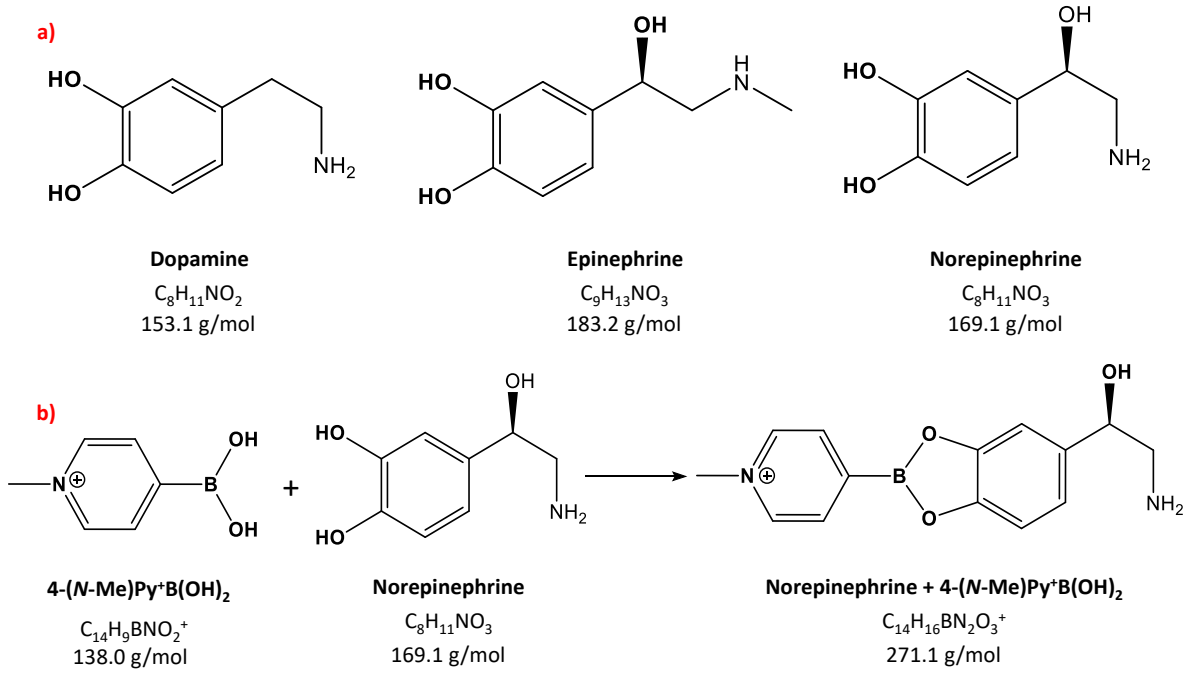

Figure 3. Molecular structures of catecholamines a) dopamine, epinephrine, and norepinephrine. b) Reaction scheme for derivatization of norepinephrine with 4-(N-methyl) pyridinium boronic acid (4-(*N*-Me)$Py^+B(OH)_2$) which yields the corresponding boronate ester via the boronic acid reaction with the catechol group.

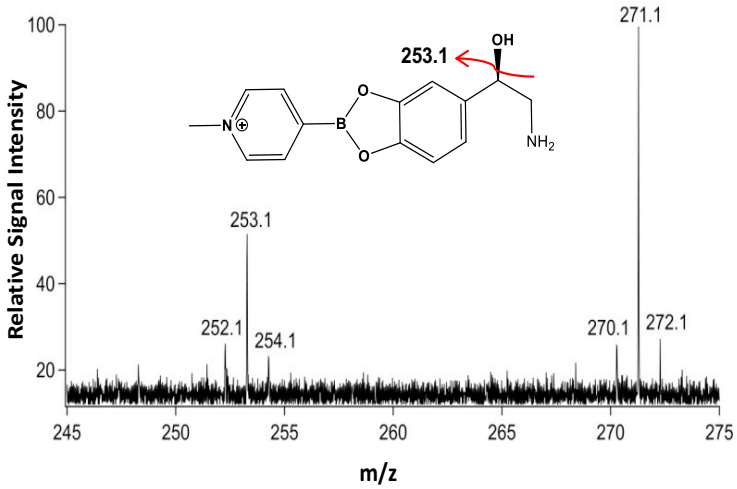

Figure 4. LDI-ToF-MS spectrum of epinephrine derivatized with 4-(N-methyl) pyridinium boronic acid (4-(*N*-Me)$Py^+B(OH)_2$). The ion peaks of resulting boronate ester complex, norepinephrine-4-(*N*-Me)$Py^+B(OH)_2$ (m/z 271.1) and its fragment ion, norepinephrine-4-(*N*-Me)$Py^+B(OH)_2$ ($[M-H_2O]^+$, m/z

253.1) were observed. The isotopic patterns were in agreement with theoretical ones. Fragmentation pathway for dehydration was proposed.

Figure 3b indicates the product of the reaction between (4-(*N*-Me)$Py^{+}B(OH)_2$ and epinephrine which yielded two ions at m/z 271.1 and m/z 253.1 in LDI-ToF-MS spectrum representing the boronate ester compound and its fragment ion, respectively (Figure 4). The isotopic patterns of both the species are in agreement with the theoretical ones which highlight that the boron atom reflects a unique isotopic distribution on the derivatized epinephrine.

Chemical Derivatization of Catecholamines in Porcine Adrenal Gland Tissue using 4-borono-N-methylpyridinium Iodide for ToF-SIMS and LDI-ToF Mass Spectrometry Imaging.

Adrenal glands are endocrine glands which produce, store and deliver variety of hormones and catecholamines by chromaffin cells in the adrenal medulla which regulate stress response in several mammalian species. H&E staining of porcine adrenal gland tissue sections revealed the adrenal cortex, the inner medulla and the capsule (Figure 4). The medulla is the innermost part of the adrenal gland, consisting of cells that secrete epinephrine (a.k.a. adrenaline), norepinephrine (a.k.a. noradrenaline), and a small amount of dopamine in response to stimulation by sympathetic preganglionic neurons. Two types of chromaffin cells, epinephrine-storing (E) and norepinephrine-storing (N), have different spatial organization within the central medulla.[55,56] Peripheral areas in the medulla of the porcine adrenal gland are occupied with E cells and central regions with NE cells.[57] These areas can be seen by H&E staining of porcine adrenal gland (Figure 4b, c, d) where the peripheral layer (Figure 4d) was rich in blood vessels compared to the central layer (Figure 4c).

Adrenal glands were chosen to test the feasibility of our chemical derivatization approach for on-tissue chemical derivatization and imaging mass spectrometry so that comparison can be made with previous reports of different strategies for the detection and imaging of these molecules. Previously, Wu et al. performed desorption electrospray ionization imaging mass

spectrometry (DESI-IMS) in porcine adrenal gland and imaged epinephrine and norepinephrine along with several lipids at 200 μm spatial resolution. Detection of dopamine in adrenal medulla was not reported which is probably due to its lower abundance.[58] Another approach reported by Manier et al. was the chemical derivatization of catecholamines in porcine adrenal gland using 4-hydroxy-3-methoxy-cinnamaldehyde (CA) where carbonyl of CA forms a stable Schiff base with amine moiety in catecholamines and the resulting complex can be detected and imaged with MALDI-IMS using ferulic acid as the matrix.[44] Underivatized MALDI-IMS analysis using HCCA resulted in isobaric interferences and low detection sensitivity compared to derivatized experiments.[44]

We devised a strategy for the derivatization of catecholamines where the resulting complex would be detected with both LDI-MS and SIMS techniques due to the permanent cationic charge on the pyridinium in 4-(*N*-methyl) pyridinium boronic acid (4-(*N*-Me)$Py^{+}B(OH)_2$) which facilitates sensitive detection of the derivatized catecholamines. This is particularly advantageous considering the possibility of re-neutralization of the ions of analytes and/or the derivatized analytes (lacking a permanent charge) in the competing gas phase reactions in matrix-assisted laser desorption plumes. The derivitazing agent reported here also removes the need for addition of a second “matrix” in the LDI analysis.

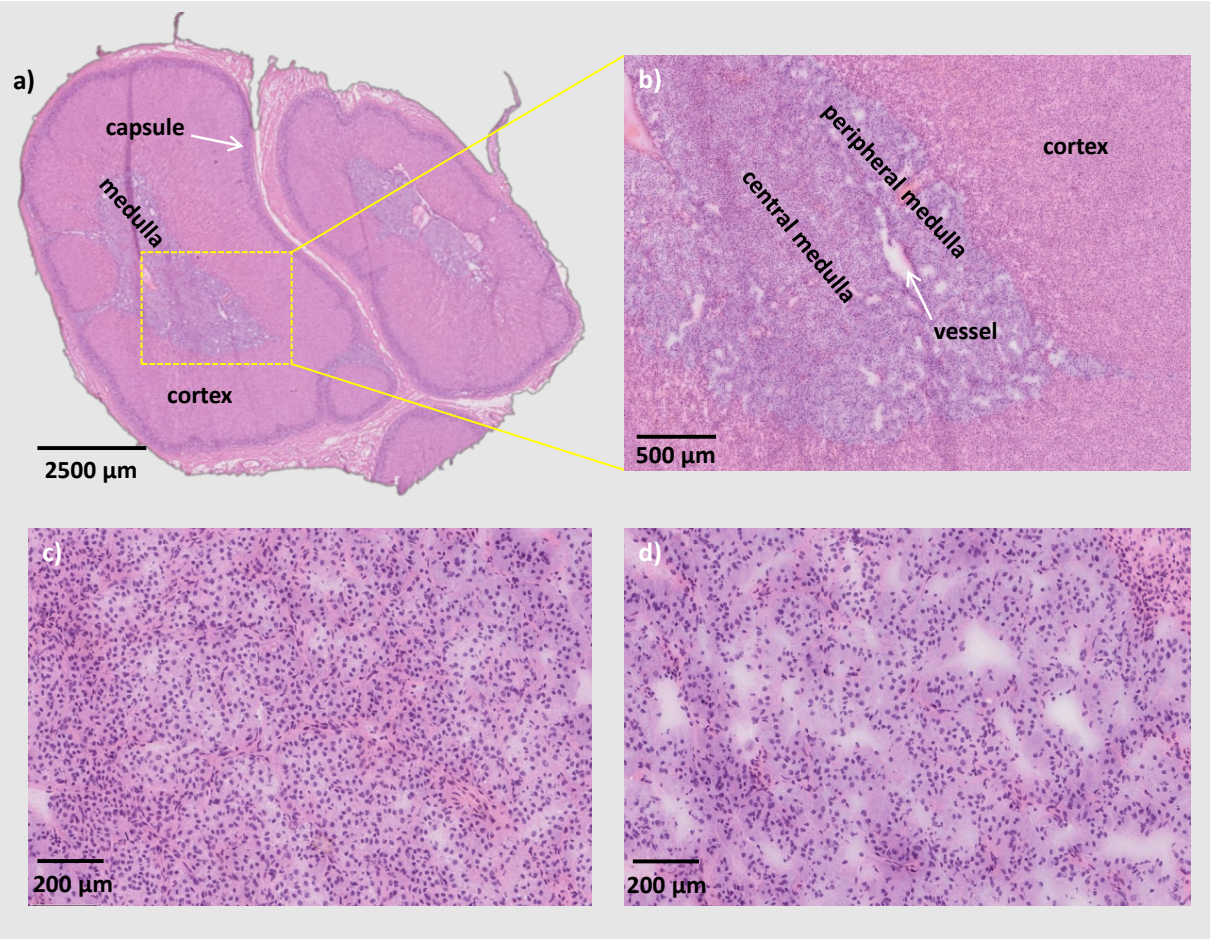

Figure 5. Optical Images of a) H&E stained pig adrenal gland tissue section reveals the histological features including the capsule, adrenal medulla and cortex. b) Zoomed medullar area and adjacent cortical region indicating different layers of cells in the central and peripheral medulla along with zoomed image of cells in c) central medulla and d) peripheral medulla.

On-tissue chemical derivatization was performed with a temperature-controlled sprayer (TM Sprayer, HTX Technologies, Carrboro, NC) to minimize the risk of analyte delocalization. LDI-ToF-IMS experiments were performed on the whole porcine adrenal gland tissue section at 100 µm spatial resolution. Fragment ions of the dopamine-4-(*N*-Me)$Py^+B(OH)_2$ ($[M\text{-}NH_2]^+$, m/z 238.1), norepinephrine-4-(*N*-Me)$Py^+B(OH)_2$ ($[M\text{-}H_2O]^+$, m/z 253.1) and epinephrine-4-(*N*-Me)$Py^+B(OH)_2$ ($[M\text{-}H_2O]^+$, m/z 267.1) were visualized in the porcine adrenal medulla whereas no catecholamines were observed in the adrenal cortex (Figure 6). As no additional matrix was added, the signals arise almost exclusively from molecules that have been derivatized and so

there was a low background signal and no isobaric spectral interferences. This facilitated specific detection and imaging of catecholamines in adrenal medulla (Figure 6). Further, the unique isotopic pattern of the boron atom (^{10}B and ^{11}B natural abundance of 19.9 and 80.1%, respectively)[52] reflected a selective isotopic pattern of the ion peaks of the derivatized catecholamines on tissue. Spatial distributions of norepinephrine-4-(*N*-Me)$Py^+B(OH)_2$ (m/z 253.1) and epinephrine-4-(*N*-Me)$Py^+B(OH)_2$ (m/z 267.1) were in line with the previous results obtained with immunohistochemical studies coupled to light or electron microscopy that highlight the specific locations of the N and NE chromaffin cells.[56,57] The ion of norepinephrine-4-(*N*-Me)$Py^+B(OH)_2$ (m/z 253.1) was most strongly localized to central regions in the porcine adrenal medulla, whereas epinephrine-4-(*N*-Me)$Py^+B(OH)_2$ (m/z 267.1) was distributed in the periphery (Figure 6c,d,e). Additionally, the ion of dopamine-4-(*N*-Me)$Py^+B(OH)_2$ (m/z 238.1) was observed across the whole adrenal medulla in the porcine adrenal gland (Figure 6b).

Interestingly, in the LDI-IMS analysis of tissue sections, only fragment ions of the derivatized catecholamines were detected whereas the feasibility experiments performed by mixing the standard catecholamines and 4-(*N*-Me)$Py^+B(OH)_2$ revealed the intact ions; norepinephrine-4-(*N*-Me)$Py^+B(OH)_2$ (m/z 271.1), epinephrine-4-(*N*-Me)$Py^+B(OH)_2$ (m/z 285.1) and dopamine-4-(*N*-Me)$Py^+B(OH)_2$ (m/z 255.1) along with the fragment ions. We postulate that at low concentrations (within tissue sections) the laser desorption ionization works mainly by the interaction of the laser light directly with the catecholamine-4-(*N*-Me)$Py^+B(OH)_2$ complex whereas at high-concentrations (feasibility experiments with standards), the laser desorption ionization can desorb the surrounding catecholamine-4-(*N*-Me)$Py^+B(OH)_2$ complex molecules (without fragmenting) along with the ones directly laser irradiated (likely fragmented) and desorbed.

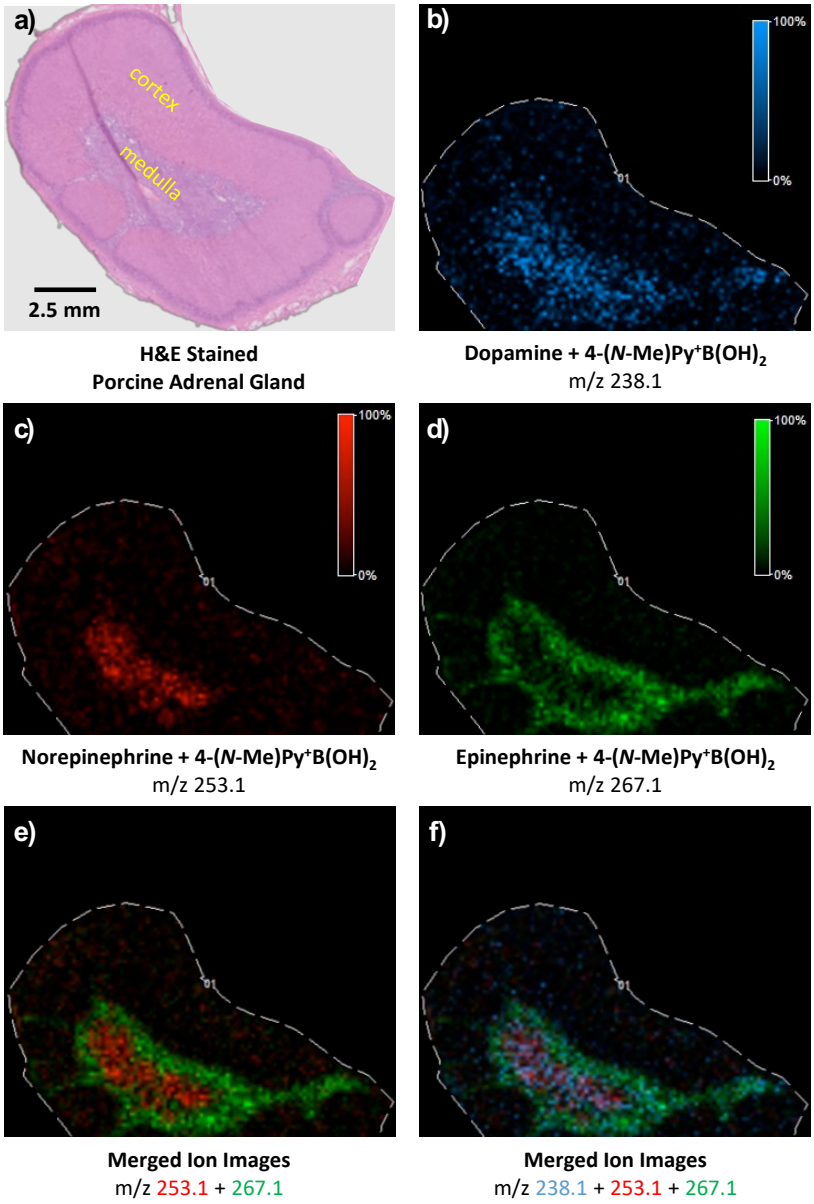

Figure 6. LDI-ToF-IMS analysis of derivatized catecholamines with 4-(*N*-methyl) pyridinium boronic acid (4-(*N*-Me)$Py^+B(OH)_2$) in porcine adrenal gland tissue section. a) Microscopy image of H&E stained consecutive porcine adrenal gland tissue section reveals histological features including adrenal medulla and adrenal cortex. Ion images (100 µm spatial resolution) diagnostic fragment ions of derivatized catecholamines; b) dopamine-4-(*N*-Me)$Py^+B(OH)_2$ (m/z 238.1), c) norepinephrine-4-(*N*-Me)$Py^+B(OH)_2$ (253.1), d) epinephrine-4-(*N*-Me)$Py^+B(OH)_2$ (m/z 267.1), e) merged ion images of norepinephrine-4-(*N*-Me)$Py^+B(OH)_2$ (m/z 253.1) in red and epinephrine-4-(*N*-Me)$Py^+B(OH)_2$ (m/z 267.1) in green. f) merged ion images of dopamine-4-(*N*-Me)$Py^+B(OH)_2$ (m/z 238.1) in blue, norepinephrine-4-(*N*-Me)$Py^+B(OH)_2$ (m/z 253.1) in red and epinephrine-4-(*N*-Me)$Py^+B(OH)_2$ (m/z 267.1) in green.

While the specific properties of the derivatizing agent were tailored to LDI-MS experiments (stable charge and UV absorption), it was envisaged that there might also benefits for ToF-SIMS analysis. The addition of a stable charge can aid detection and the shift in molecular mass may move the target analytes to a "cleaner" m/z range and reduce isobaric interferences. ToF-SIMS imaging analysis performed on a consecutive tissue section on the same ITO coated glass slide. The newly developed gas cluster ion beams (GCIBs) that comprise clusters of often several thousand argon atoms and which are demonstrated to enhance the intact molecular ion species (such as lipids, small peptides with less damage accumulation in depth profiling compared to C_{60}^+) in high mass ranges at high spatial-resolutions.[8,32,59] A region of porcine adrenal gland tissue section containing adrenal cortex and adrenal medulla was analyzed with GCIB-ToF-SIMS imaging (30 µm per pixel) (Figure 6). Intact derivatized ions and fragment ions of catecholamines were detected in adrenal medulla without no observable isobaric interference from the tissue components. Figure 7 contains the ion images of a sphingomyelin lipid (SM (36:1), $[M+Na]^+$ at m/z 753.5), norepinephrine-4-(*N*-Me)$Py^+B(OH)_2$ (m/z 271.1), epinephrine-4-(*N*-Me)$Py^+B(OH)_2$ (m/z 285.1), dopamine-4-(*N*-Me)$Py^+B(OH)_2$ (m/z 255.1) and a fragment ion from epinephrine/norepinephrine-4-(*N*-Me)$Py^+B(OH)_2$ (m/z 240.1, see Figure 8 and later discussion) in porcine adrenal gland.

Compared to LDI-MS analysis, GCIB-ToF-SIMS provided a more sensitive detection and gentler ejection of the derivatized catecholamines with 4-(*N*-Me)$Py^+B(OH)_2$. The intact molecular ions of catecholamines-4-(*N*-Me)$Py^+B(OH)_2$ complexes were also detected and were more abundant compared to the fragment ions detected in the LDI-MS. While GCIB-ToF-SIMS still provided background signals, the derivatization via boronate ester formation moved the SIMS ion peaks of derivatized-catecholamines from major isobaric interferences such as the abundant phosphocholine head group which overlaps with the underivatized epinephrine signal at m/z 184.1.

Spatial distributions of epinephrine, norepinephrine and dopamine ions were in line with the LDI-ToF-IMS analysis. Ions from norepinephrine-4-(*N*-Me)$Py^+B(OH)_2$ (m/z 271.1) were

detected in central regions in the porcine adrenal medulla, whereas epinephrine-4-(*N*-Me)$Py^+B(OH)_2$ (m/z 285.3) was distributed in peripheral regions (Figure 6c,e,g,h). On the other hand, the ion of dopamine-4-(*N*-Me)$Py^+B(OH)_2$ (m/z 255.1) was observed across the whole adrenal medulla in the porcine adrenal gland (Figure 6d,g).

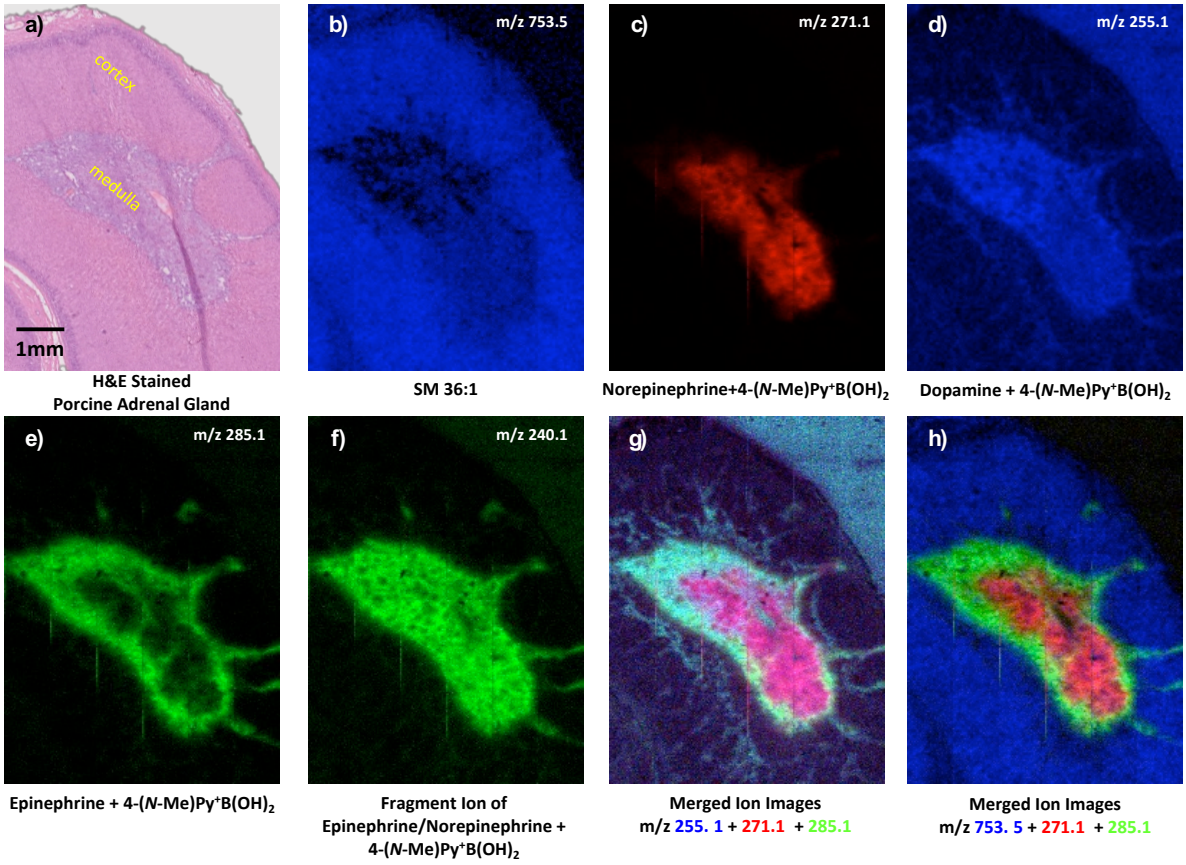

Figure 7. GCIB-ToF-SIMS imaging (30 µm per pixel) analysis of derivatized catecholamines with 4-(N-methyl) pyridinium boronic acid (4-(*N*-Me)$Py^+B(OH)_2$) in porcine adrenal gland tissue section. a) Microscopy image of H&E stained consecutive porcine adrenal gland tissue section reveals histological features including adrenal medulla and adrenal cortex. Ion images of b) sphingomyelin lipid (SM(36:1), $[M+Na]^+$ m/z 753.5), c) norepinephrine-4-(*N*-Me)$Py^+B(OH)_2$ (m/z 271.1), d) dopamine-4-(*N*-Me)$Py^+B(OH)_2$ (m/z 255.1), e) epinephrine-4-(*N*-Me)$Py^+B(OH)_2$ (m/z 285.1), f) fragment ion of epinephrine/norepinephrine-4-(*N*-Me)$Py^+B(OH)_2$, g) merged ion images of norepinephrine-4-(*N*-Me)$Py^+B(OH)_2$ (m/z 271.1) in red , epinephrine-4-(*N*-Me)$Py^+B(OH)_2$ (m/z 285.1) in green and dopamine-4-(*N*-Me)$Py^+B(OH)_2$ (m/z 255.1) in blue. h) merged ion images of sphingomyelin (SM 36:1, $[M+Na]^+$ m/z 753.5) in blue, norepinephrine-4-(*N*-Me)$Py^+B(OH)_2$ (m/z 271.1) in red and epinephrine-4-(*N*-

Me)$Py^+B(OH)_2$ (m/z 285.1) in green. Image dimensions: 5760 x 7680 μm^2. Primary ion dose: 1.14 x 10^{11} ions/cm^2.

Although chemical derivatization and the specific isotopic pattern improve the sensitivity and specificity of the detection of catecholamines, we performed validation of the derivatized catecholamines whereby on-tissue MS/MS analysis of derivatized catecholamines was performed using CID-ToF-ToF-SIMS in positive ion mode. For example, CID-ToF-ToF-SIMS-MS/MS analysis of derivatized epinephrine with 4-(N-methyl) pyridinium boronic acid (4-(*N*-Me)$Py^+B(OH)_2$) revealed specific fragments of the resulting boronate ester complex (Figure 7a). The fragment ion (m/z 240.1) which was visualized in adrenal medulla was observed as a product ion in the MS/MS analysis of the epinephrine/norepinephrine-4-(*N*-Me)$Py^+B(OH)_2$ boronate ester complexes and was further analyzed as a precursor ion with CID-ToF-ToF-SIMS (Figure 8b).

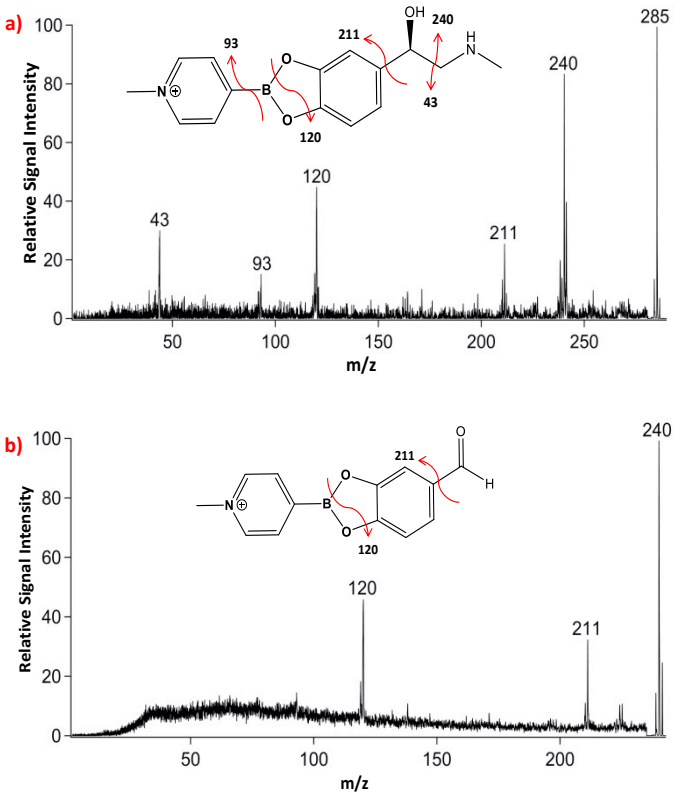

Figure 8. On tissue CID-ToF-ToF-SIMS-MS/MS analysis of derivatized epinephrine with 4-(*N*-methyl) pyridinium boronic acid (4-(*N*-Me)$Py^+B(OH)_2$) in the medulla region of porcine adrenal gland. a) MS/MS spectra and proposed fragmentation pathways for epinephrine-4-(*N*-Me)$Py^+B(OH)_2$ (m/z 285.1) and b) the fragment ion at m/z 240.1 obtained from the corresponding regions in the porcine adrenal gland after the GCIB-ToF-SIMS imaging experiment using CID-ToF-ToF-SIMS in positive ion mode. The product ion regions of the MS/MS spectra were multiplied up by a factor of 50.

High-spatial resolution is an important objective of imaging mass spectrometry. Although recent advancements in the instrumentation and laser focusing technologies allow subcellular spatial resolution (~1 μm) MALDI-IMS experiments on tissue sections[60,61], the best spatial resolution that can be obtained with the MALDI-ToF-IMS instrument in our lab (Bruker UltrafleXtreme, Smartbeam-II™ laser) is 10 μm (without resorting to oversampling). As primary ions emitted in vacuum can be easily focused by electrostatic lenses, ion beam spot sizes can go down to 10s of nm in favorable cases in IMS analysis although for detection of (small, abundant) molecular ions 0.5 – 1 μm is normal. Gas cluster ion beams (GCIBs) have been introduced that comprise clusters of often several thousand argon atoms and which are demonstrated to enhance the intact molecular ion species in high mass ranges (such as cardiolipins[62] and gangliosides[8]) at high spatial-resolutions but limited, so far, to around 1-3 μm.[8,32] We used a GCIB for the imaging of catecholamines derivatized with 4-(*N*-methyl) pyridinium boronic acid. Intact ions of resulting boronate ester complexes of dopamine, epinephrine and norpepinephrine were visualized in porcine adrenal medulla at 3 μm per pixel spatial resolution (Figure 9).

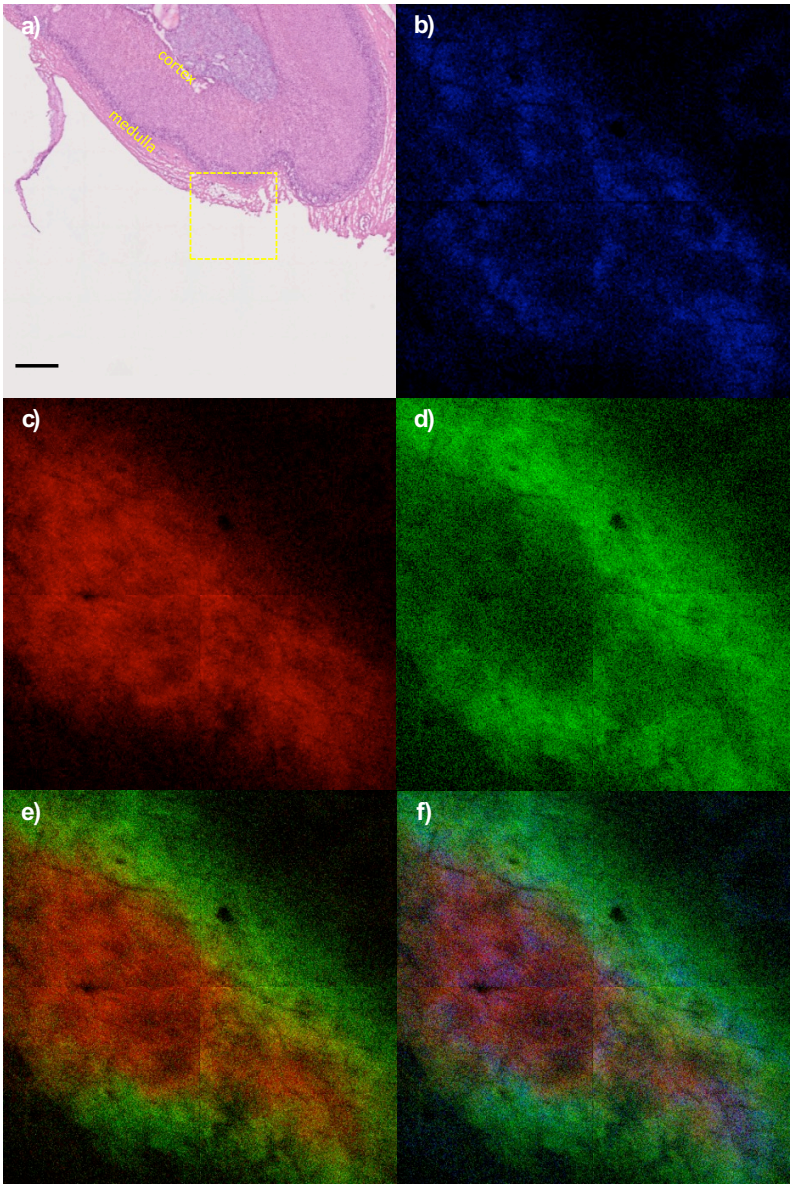

Figure 9. High spatial resolution GCIB-ToF-SIMS imaging (3 µm per pixel) analysis of derivatized catecholamines with 4-(N-methyl) pyridinium boronic acid (4-(*N*-Me)$Py^+B(OH)_2$) in porcine adrenal gland tissue section. a) Microscopy image of H&E stained consecutive porcine adrenal gland tissue section reveals histological features including adrenal medulla and adrenal cortex. Ion images of b) dopamine-4-(*N*-Me)$Py^+B(OH)_2$ (m/z 255.1), c) norepinephrine-4-(*N*-Me)$Py^+B(OH)_2$ (m/z 271.1), d) epinephrine-4-(*N*-Me)$Py^+B(OH)_2$ (m/z 285.1), e) merged ion images of norepinephrine-4-(*N*-Me)$Py^+B(OH)_2$ (m/z 271.1) in red , epinephrine-4-(*N*-Me)$Py^+B(OH)_2$ (m/z 285.1) in green, f) merged ion images of norepinephrine-4-(*N*-Me)$Py^+B(OH)_2$ (m/z 271.3) in red , epinephrine-4-(*N*-Me)$Py^+B(OH)_2$ (m/z 285.1) in green and dopamine-4-(*N*-Me)$Py^+B(OH)_2$ (m/z 255.1) in blue. Image dimensions: 1536 x 1536 μm^2. Primary ion dose: 2.78 x 10^{12} ions/cm^2. Scale bar: panel a, 2200 µm.

CONCLUSIONS

A strategy to derivatize the catecholamines from their catechol-side (*ortho* isomer of dihydroxybenzene) by utilizing the high-affinity binding of boronic acids with diol moieties through boronate ester formation has been devized and tested using LDI-MS and SIMS. 4-(*N*-methyl) pyridinium boronic acid iodide was designed and synthesized as a derivatization agent for catecholamines. The permanent charge in 4-(*N*-methyl) pyridinium boronic acid provided sensitive ionization of catecholamines upon derivatization for both SIMS and LDI desorption/ionization techniques. The unique isotopic pattern reflected a selective isotopic pattern for the ions of derivatized catecholamines. Particularly, the UV absorption maxima of boronate ester complex of 4-(*N*-methyl) pyridinium boronic acid was ~358 nm (in the solution) and this allowed use of 4-(*N*-methyl) pyridinium boronic acid as a “reactive matrix’’ for LDI-MS detection of catecholamines. The methodology was utilized to sensitively and selectively detect and localize catecholamines using both LDI-MS and GCIB-ToF-SIMS (down to 3 μm per pixel spatial resolution) in porcine adrenal gland tissue as a proof of concept for imaging mass spectrometry. The feature of this technique which is requiring no matrix molecule for desorption/ionization of the derivatized catecholamines resulted in minimum background signals with LDI-MS, while SIMS still resulted in background signals. However, derivatization via boronate ester formation moved the SIMS ion peaks of derivatized catecholamines from major isobaric interferences such as the abundant phosphocholine head group (m/z 184.1). Secondary ion ejection with GCIB resulted in ion peaks of intact derivatized catecholamines dominantly (likely due to its gentle ejection feature) in IMS analysis, whereas LDI resulted in only fragment ions (dehydration or deamination) in porcine adrenal gland tissue sections.

This methodology can be a powerful approach for the selective and sensitive ionization/detection and spatial localization of diol-containing molecules such as aminols, vic-diols, saccharides and glycans along with catecholamines in tissue sections with both SIMS and LDI/MALDI-MS techniques.

ASSOCIATED CONTENT

Supporting Information.

Detailed information for the synthesis of 4-(*N*-methyl) pyridinium boronic acid Iodide compound. NMR spectra for the product and intermadiate products of the synthesis. High-resolution mass spectrometry (HRMS) spectra for synthesized 4-(*N*-methyl) pyridinium boronic acid Iodide. Reaction schemes and LDI-ToF-MS spectra for the reaction of catechol, dopamine, epinpehrine and norepinephrine with 4-(*N*-methyl) pyridinium boronic acid. UV-VIS spectroscopy analysis 4-(N-methyl) pyridinium boronic acid pinacol ester (4-(*N*-Me)$Py^{+}B(OC_3H_6)_2$).

AUTHOR INFORMATION

***Corresponding Author**

John S. Fletcher

Department of Chemistry and Molecular Biology, University of Gothenburg, Analytical Chemistry, SE-412 96, Gothenburg, Sweden

john.fletcher@chem.gu.se;

+46-76 622 91 05

ORCID:

Ibrahim Kaya: 0000-0003-3345-5602

John S. Fletcher: 0000-0002-9418-8571

Per Malmberg: 0000-0002-6487-7851

Andrew G. Ewing: 0000-0002-2084-0133

FUNDING This study was financially supported by the Swedish Government under the LUA/ALF Agreement (grant #71570, E.J.,S.L.), Sahlgrenska University Hospital (grant #83030,

E.J.,S.L.), the Swedish Research Council VR (grant #2015-05274, P.M. and grant #2016-04669, J.S.F).

NOTES Authors declare no competing financial interest.

ACKNOWLEDGEMENTS MALDI-IMS and GCIB-ToF-SIMS-IMS experiments were performed in the go:IMS imaging MS laboratory at the University of Gothenburg/Chalmers University of Technology (www.go-ims.gu.se). HRMS experiments were performed at Chalmers Mass Spectrometry Infrastructure (CMSI) directed by Otto Savolainen. Authors thank to Maria Vizcaino from CMSI for performing HRMS experiments.

LIST OF ABBREVIATIONS ACN, acetonitrile; GCIB, gas cluster ion beams; FT-ICR, fourier-transform ion cyclotron resonance; LDI, laser desorption/ionization; SIMS, secondary ion mass spectrometry; MALDI, matrix-assissted laser desorption/ionization, DESI, desorption electrospray ionization; IMS, imaging mass spectrometry; NT, neurotransmitter; ToF, time of flight; H&E, hematoxylin and eosin; UV-VIS, ultraviolet-visible; HRMS, High-resolution mass spectrometry; CID, collision-induced dissociation; NT, neurotransmitters.

REFERENCES

(1) Reuter, H. *Nature* **1983**, *301*, 569-574.
(2) Lauder, J. M. *Trends in neurosciences* **1993**, *16*, 233-240.
(3) MacDonald, S. W.; Nyberg, L.; Bäckman, L. *Trends in neurosciences* **2006**, *29*, 474-480.
(4) Caprioli, R. M.; Farmer, T. B.; Gile, J. *Analytical chemistry* **1997**, *69*, 4751-4760.
(5) Spraggins, J. M.; Rizzo, D. G.; Moore, J. L.; Rose, K. L.; Hammer, N. D.; Skaar, E. P.; Caprioli, R. M. *Journal of the American Society for Mass Spectrometry* **2015**, *26*, 974-985.
(6) Kaya, I.; Brinet, D.; Michno, W.; Başkurt, M.; Zetterberg, H.; Blenow, K.; Hanrieder, J. r. *ACS chemical neuroscience* **2017**, *8*, 2778-2790.
(7) Ogrinc Potočnik, N.; Fisher, G. L.; Prop, A.; Heeren, R. M. *Analytical chemistry* **2017**, *89*, 8223-8227.
(8) Angerer, T. B.; Dowlatshahi Pour, M.; Malmberg, P.; Fletcher, J. S. *Analytical chemistry* **2015**, *87*, 4305-4313.

(9) Kaya, I.; Michno, W.; Brinet, D.; Iacone, Y.; Zanni, G.; Blennow, K.; Zetterberg, H.; Hanrieder, J. r. *Analytical Chemistry* **2017**, *89*, 4685-4694.
(10) Cornett, D. S.; Frappier, S. L.; Caprioli, R. M. *Analytical chemistry* **2008**, *80*, 5648-5653.
(11) McDonnell, L. A.; Heeren, R. *Mass spectrometry reviews* **2007**, *26*, 606-643.
(12) Vickerman, J. C. *Analyst* **2011**, *136*, 2199-2217.
(13) Norris, J. L.; Caprioli, R. M. *Chemical reviews* **2013**, *113*, 2309-2342.
(14) Esteve, C.; Tolner, E. A.; Shyti, R.; van den Maagdenberg, A. M.; McDonnell, L. A. *Metabolomics* **2016**, *12*, 30.
(15) Shanta, S. R.; Kim, T. Y.; Hong, J. H.; Lee, J. H.; Shin, C. Y.; Kim, K.-H.; Kim, Y. H.; Kim, S. K.; Kim, K. P. *Analyst* **2012**, *137*, 5757-5762.
(16) Shariatgorji, M.; Nilsson, A.; Goodwin, R. J.; Svenningsson, P.; Schintu, N.; Banka, Z.; Kladni, L.; Hasko, T.; Szabo, A.; Andren, P. E. *Analytical chemistry* **2012**, *84*, 7152-7157.
(17) Soltwisch, J.; Jaskolla, T. W.; Hillenkamp, F.; Karas, M.; Dreisewerd, K. *Analytical chemistry* **2012**, *84*, 6567-6576.
(18) Niehaus, M.; Schnapp, A.; Koch, A.; Soltwisch, J.; Dreisewerd, K. *Analytical Chemistry* **2017**, *89*, 7734-7741.
(19) Dreisewerd, K. *Chemical reviews* **2003**, *103*, 395-426.
(20) Maharrey, S.; Bastasz, R.; Behrens, R.; Highley, A.; Hoffer, S.; Kruppa, G.; Whaley, J. *Appl. Surf. Sci.* **2004**, *231*, 972-975.
(21) Smith, D. F.; Robinson, E. W.; Tolmachev, A. V.; Heeren, R. M.; Paša-Tolić, L. *Analytical chemistry* **2011**, *83*, 9552-9556.
(22) Soltwisch, J.; Kettling, H.; Vens-Cappell, S.; Wiegelmann, M.; Müthing, J.; Dreisewerd, K. *Science* **2015**, aaa1051.
(23) Ellis, S.; Soltwisch, J.; Paine, M.; Dreisewerd, K.; Heeren, R. *Chemical Communications* **2017**, *53*, 7246-7249.
(24) Passarelli, M. K.; Pirkl, A.; Moellers, R.; Grinfeld, D.; Kollmer, F.; Havelund, R.; Newman, C. F.; Marshall, P. S.; Arlinghaus, H.; Alexander, M. R. *Nature methods* **2017**, *14*, 1175.
(25) Springsteen, G.; Wang, B. *Tetrahedron* **2002**, *58*, 5291-5300.
(26) Axthelm, J. r.; Askes, S. H.; Elstner, M.; Görls, H.; Bellstedt, P.; Schiller, A. *Journal of the American Chemical Society* **2017**, *139*, 11413-11420.
(27) Whyte, G. F.; Vilar, R.; Woscholski, R. *Journal of chemical biology* **2013**, *6*, 161-174.
(28) Maue, M.; Schrader, T. *Angewandte Chemie* **2005**, *117*, 2305-2310.
(29) Maki, T.; Ishihara, K.; Yamamoto, H. *Tetrahedron* **2007**, *63*, 8645-8657.
(30) Fletcher, J. S.; Rabbani, S.; Henderson, A.; Blenkinsopp, P.; Thompson, S. P.; Lockyer, N. P.; Vickerman, J. C. *Anal. Chem.* **2008**, *80*, 9058-9064.
(31) Hill, R.; Blenkinsopp, P.; Thompson, S.; Vickerman, J.; Fletcher, J. S. *Surf Interface Anal* **2011**, *43*, 506-509.
(32) Angerer, T. B.; Blenkinsopp, P.; Fletcher, J. S. *Int. J. Mass Spectrom.* **2015**, *377*, 591-598.
(33) Angerer, T. B.; Magnusson, Y.; Landberg, G.; Fletcher, J. S. *Anal. Chem.* **2016**, *88*, 11946-11954.
(34) Wehrli, P. M.; Angerer, T. B.; Farewell, A.; Fletcher, J. S.; Gottfries, J. *Anal. Chem.* **2016**, *88*, 8680-8688.
(35) Munem, M.; Zaar, O.; Nilsson, K. D.; Neittaanmaki, N.; Paoli, J.; Fletcher, J. S. *Biointerphases* **2018**, *13*.
(36) Sämfors, S.; Ståhlman, M.; Klevstig, M.; Borén, J.; Fletcher, J. S. *Int. J. Mass Spectrom.* **2017**.
(37) Tian, H.; Sparvero, L. J.; Amoscato, A. A.; Bloom, A.; Bayir, H.; Kagan, V. E.; Winograd, N. *Anal. Chem.* **2017**, *89*, 4611-4619.
(38) Fletcher, J. S.; Kotze, H. L.; Armitage, E. G.; Lockyer, N. P.; Vickerman, J. C. *Metabolomics* **2013**, *9*, 535-544.
(39) Wehrli, P. M.; Lindberg, E.; Angerer, T. B.; Wold, A. E.; Gottfries, J.; Fletcher, J. S. *Surf. Interface Anal.* **2014**, *46*, 173-176.
(40) Phan, N. T. N.; Munem, M.; Ewing, A. G.; Fletcher, J. S. *Anal. Bioanal. Chem.* **2017**, *409*, 3923-3932.

(41) Suckau, D.; Resemann, A.; Schuerenberg, M.; Hufnagel, P.; Franzen, J.; Holle, A. *Analytical and bioanalytical chemistry* **2003**, *376*, 952-965.
(42) Optimizing, U. *Journal of Mass Spectrometry* **2006**, *41*, 705-716.
(43) Shariatgorji, M.; Nilsson, A.; Källback, P.; Karlsson, O.; Zhang, X.; Svenningsson, P.; Andren, P. E. *Journal of the American Society for Mass Spectrometry* **2015**, *26*, 934-939.
(44) Manier, M. L.; Spraggins, J. M.; Reyzer, M. L.; Norris, J. L.; Caprioli, R. M. *Journal of Mass Spectrometry* **2014**, *49*, 665-673.
(45) Shariatgorji, M.; Nilsson, A.; Goodwin, R. J.; Källback, P.; Schintu, N.; Zhang, X.; Crossman, A. R.; Bezard, E.; Svenningsson, P.; Andren, P. E. *Neuron* **2014**, *84*, 697-707.
(46) Diesner, M.; Neupert, S. *Analytical chemistry* **2018**.
(47) Karas, M.; Glückmann, M.; Schäfer, J. *Journal of mass spectrometry* **2000**, *35*, 1-12.
(48) Karas, M.; Krüger, R. *Chemical reviews* **2003**, *103*, 427-440.
(49) Knochenmuss, R. *Analyst* **2006**, *131*, 966-986.
(50) Delcorte, A.; Garrison, B. *The Journal of Physical Chemistry B* **2000**, *104*, 6785-6800.
(51) Wallingford, R. A.; Ewing, A. G. *Journal of Chromatography A* **1988**, *441*, 299-309.
(52) Nishikaze, T.; Kawabata, S. i.; Tanaka, K. *Journal of Mass Spectrometry* **2013**, *48*, 1005-1009.
(53) Monopoli, A.; Calvano, C.; Nacci, A.; Palmisano, F. *Chemical Communications* **2014**, *50*, 4322-4324.
(54) Pizer, R.; Babcock, L. *Inorganic Chemistry* **1977**, *16*, 1677-1681.
(55) Suzuki, T.; Kachi, T. *Neuroscience letters* **1994**, *176*, 217-220.
(56) Coupland, R.; HOPWOOD, D. *Nature* **1966**, *209*, 590.
(57) Suzuki, T.; Kachi, T. *The Anatomical Record: An Official Publication of the American Association of Anatomists* **1996**, *244*, 358-365.
(58) Wu, C.; Ifa, D. R.; Manicke, N. E.; Cooks, R. G. *Analyst* **2010**, *135*, 28-32.
(59) Rabbani, S.; Barber, A. M.; Fletcher, J. S.; Lockyer, N. P.; Vickerman, J. C. *Analytical chemistry* **2011**, *83*, 3793-3800.
(60) Zavalin, A.; Yang, J.; Hayden, K.; Vestal, M.; Caprioli, R. M. *Analytical and bioanalytical chemistry* **2015**, *407*, 2337-2342.
(61) Kompauer, M.; Heiles, S.; Spengler, B. *nAture methods* **2017**, *14*, 90.
(62) Tian, H.; Sparvero, L. J.; Amoscato, A. A.; Bloom, A.; Bayır, H. l.; Kagan, V. E.; Winograd, N. *Analytical chemistry* **2017**, *89*, 4611-4619.

For TOC Figure only